Characterization of fragment emission in ^{20}Ne(7–10 MeV/nucleon)+^{12}C reactions

Aparajita Dey,[1] C. Bhattacharya,[1] S. Bhattacharya,[1] S. Kundu,[1] K. Banerjee,[1] S. Mukhopadhyay,[1] D. Gupta,[1] T. Bhattacharjee,[1] S. R. Banerjee,[1] S. Bhattacharyya,[1] T. K. Rana,[1] S. K. Basu,[1] R. Saha,[1] K. Krishan,[1,*] A. Mukherjee,[1,†] D. Bandopadhyay,[1,‡] and C. Beck[2]

[1]*Variable Energy Cyclotron Centre, Sector 1, Block AF, Bidhan Nagar, Kolkata 700 064, India.*

[2]*Institut Pluridisciplinaire Hubert Curien, UMR7500, CNRS-IN2P3 et Universite Louis Pasteur, 23, Rue du Loess, B.P. 28, F-67037, Strasbourg Cedex 2, France*

(Received 30 June 2007; published 21 September 2007)

The inclusive energy distributions of the complex fragments ($3 \leqslant Z \leqslant 7$) emitted from the bombardment of ^{12}C by ^{20}Ne beams with incident energies between 145 and 200 MeV have been measured in the angular range $10^\circ \leqslant \theta_{lab} \leqslant 50^\circ$. Damped fragment yields in all the cases have been found to have the characteristic of emission from fully energy equilibrated composites. The binary fragment yields are compared with the standard statistical model predictions. Whereas Li and Be fragments yields are in agreement with statistical-model calculations, enhanced yields of entrance channel fragments ($5 \leqslant Z \leqslant 7$) indicate the survival of orbiting-like process in ^{20}Ne+^{12}C system at these energies.

DOI: 10.1103/PhysRevC.76.034608 PACS number(s): 25.70.Jj, 24.60.Dr, 25.70.Lm

I. INTRODUCTION

Several experiments have been done in recent years to understand the mechanism of complex fragment emission in low-energy ($E_{lab} \lesssim 10$ MeV/nucleon) light heavy-ion ($A_{projectile}+A_{target} \lesssim 60$) reactions [1–17]. The origin of these fragments extends from quasi-elastic (QE)/ projectile breakup [2,3], deep-inelastic (DI) transfer and orbiting [4,6,12–16], to fusion-fission (FF) [18–23] processes; in some cases the structure of the nuclei has been found to play an important role. In most of the reactions studied, the observed fully energy-damped yields of the fragments have been successfully explained in terms of fusion-fission (FF) mechanism [18–23]. However, the reactions involving α-cluster nuclei (e.g., ^{20}Ne+^{12}C [12,13], ^{24}Mg+^{12}C [16], ^{28}Si+^{12}C [14,24], etc.) deserved special attention, where the observations of large enhancement in yield and/or resonance-like excitation function in a few outgoing channels have been indicative of a competitive role played by the deep-inelastic orbiting mechanism [12–15]. In the FF mechanism, a completely equilibrated compound nucleus (CN) is formed, which decays into various exit channels. The decay probability is governed by the available phase space and barrier penetration probabilities for the respective decay channels. The process occurs in a similar time scale that is required for the complete relaxation of the entrance channel energy and angular momentum. However, deep inelastic orbiting may be described in terms of the formation of a long-lived, dinuclear molecular complex [15], which acts as a "door way to fusion," with a strong memory of the entrance channel. In this picture, the interacting ions are trapped in a more deformed configuration than that of the compound nucleus (trapped in the pocket of the ion-ion interaction potential due to combined effects of Coulomb and centrifugal barriers). Both orbiting and fusion-fission processes occur on similar time scale. In addition to that, for the light heavy-ion systems, the shapes of the orbiting dinuclear complexes are quite similar to the saddle and scission shapes obtained in course of evolution of the FF process. Therefore it is difficult to differentiate the signatures of the two processes.

The enhancement of fully energy damped reaction yields in light systems was first observed in the study of ^{20}Ne+^{12}C inelastic scattering at backward angles [12], where large cross sections have been observed in inelastic-scattering yields near 180°. Subsequently, orbiting was observed in ^{28}Si+^{12}C [14,24] and ^{24}Mg+^{12}C [16] reactions. Detailed study of ^{28}Si+^{12}C system revealed that, at lower bombarding energies, the excitation spectra for the ^{12}C fragments were dominated by single excitation and mutual excitations of the ^{12}C and ^{28}Si fragments, whereas at higher bombarding energies, the dominant strength for all these channels shifted to higher excitation energies [24]. For the higher bombarding energies, the most probable Q values were found to be independent of detection angles and the resulting angular distributions were found to have $d\sigma/d\Omega \propto 1/\sin\theta_{c.m.}$ like angular dependence—characteristic of a long-lived, orbiting, dinuclear complex. Similar results have been obtained for ^{20}Ne+^{12}C system [12,13], where resonance-like behavior was also found in the excitation functions for several outgoing channels, which was similar to the observation made for symmetric ^{16}O+^{16}O system [25–28]. Enhancements of large angle, binary reaction yields have also been observed in somewhat heavier ^{28}Si+^{28}Si, ^{24}Mg+^{24}Mg systems [1], where significant non resonant background yield was observed at higher excitation energies. The general pattern which unfolds from these studies clearly suggests that the enhancements are manifestations of dynamics of damped nuclear reactions involving a large number of channels, rather than due to specific structure effect appearing only in a few select channels.

*Present address: 306, VIP Enclave, VIP Road, Kolkata 700 059, India.

†Present address: Saha Institute of Nuclear Physics, 1/AF Bidhan Nagar, Kolkata 700 064, India.

‡Present address: TRIUMF, 4004 Westbrook Mall, Vancouver, Canada V6T2A3.

The enhancement in elastic and inelastic channels may be explained in terms of a long-lived dinuclear configuration that decays back to entrance channel due to weak absorption that inhibits the orbiting configuration from spreading into compound nuclear states. However, the enhancement in the elastic channel can be explained with the assumption of weak absorption of grazing partial waves only; on the contrary, deep-inelastic orbiting phenomenon in general suggests weak absorption in the angular momentum window between the critical angular momentum of fusion, l_{cr}, and the reaction grazing angular momentum, l_{gr}. Moreover, substantial mass and charge transfer, due to the rapid mass equilibration in light systems, would also occur during the evolution of the orbiting dinuclear complex. So, the rearrangement channels are also of interest in probing the dynamics of the orbiting process involving light nuclear systems.

It is, therefore evident that, though some qualitative understanding about the phenomenon of deep-inelastic orbiting reaction, in general (i.e., correlation with number of open reaction channels [29], or, alternatively, to weak absorption) has been arrived at, precise mechanism of the process is still unknown. The deep-inelastic orbiting process has been observed in several light α-like systems, for example, ^{20}Ne+^{12}C [12,13], ^{24}Mg+^{12}C [16], ^{28}Si+^{12}C [14,24], ^{28}Si+^{16}O [30] systems, where the number of open channels are small ($\sim$10) [29]. However, ^{16}O (116 MeV)+^{28}Si reaction [6] showed different behavior so far as the shape of the energy distributions, variation of $\langle Q \rangle$ values with angle, and yields of the fragments are concerned. For a better understanding of the orbiting process, it is interesting to study how the orbiting process evolves with energy. Intuitively, survival of long-lived dinuclear configuration other than fused composite is less probable at higher excitations and there are also indications that entrance channel effect becomes smaller at higher energies [1]. Shapira *et al.* [13] made detailed study of ^{20}Ne+^{12}C system in the energy range E_{lab} = 54–81 MeV and showed that there was large enhancement of strongly damped yields, the characteristic of a long-lived orbiting ^{20}Ne+^{12}C dinuclear system. The aim of the present article was to extend the investigation on fragment yield from ^{20}Ne+^{12}C reaction at higher excitation energies, which might allow us to have a better understanding of orbiting vis-*à*-vis fusion-fission processes for ^{20}Ne+^{12}C system. If a long-lived rotating dinuclear complex is formed in these reactions, mass and charge transfer should also occur, which leads to typical deep-inelastic reaction yields. Therefore, back-angle measurements for rearrangement channels became of interest. In addition to that the excitation function measurements, for the dependence of the average total kinetic energy (E_K^{tot}) loss on bombarding energy for each binary exit channel, would provide an important probe of the dynamical properties of the long-lived dinuclear complex. With this motivation, we have studied the fragment emission spectra from the reaction ^{20}Ne+^{12}C at E_{lab} = 145, 158, 170, 180, and 200 MeV, respectively. A part of the present data has already been reported [4], which showed enhancement in yield of Carbon and Boron fragments well above the standard statistical model predictions.

The article has been arranged as follows. Section II describes the experimental procedures. In Sec. III we present the analysis of ^{20}Ne+^{12}C data. The results have been discussed in Sec IV. Finally, the summary and conclusions are presented in Sec. V.

II. EXPERIMENTS

The experiment was performed using accelerated ^{20}Ne ion beams of energies 145, 158, 170, 180, and 200 MeV, respectively, from the Variable Energy Cyclotron at Kolkata. The target used was $\sim$550 μg/cm^2 self-supporting ^{12}C. Different fragments ($5 \leqslant Z \leqslant 13$) have been detected using two solid-state [Si(SB)] telescopes ($\sim$10 μm ΔE, 300 μm E) mounted on one arm of the 91.5-cm scattering chamber. Two solid-state telescopes ($\sim$-50 μm, 100 μm ΔE [Si(SB)] and 5 mm E [Si(Li)]) were mounted on the other arm of the scattering chamber for the detection of light charged particles and light fragments ($1 \leqslant Z \leqslant 4$); the same detectors were also used as monitor detectors for normalization purposes. Typical solid angle subtended by each detector was $\sim$0.3 msr. The telescopes were calibrated using elastically scattered ^{20}Ne ion from Au, Al targets, and a Th-α source. The systematic errors in the data, arising from the uncertainties in the measurements of solid angle, target thickness and the calibration of current digitizer have been estimated to be $\approx$15%. Part of these uncertainties are due to the extrapolation procedures employed to extract the fully damped yields from the sequential decay components by the use of Monte Carlo simulations described in Sec. IV A.

III. RESULTS

A. Energy distribution

Inclusive energy distributions for various fragments ($3 \leqslant Z \leqslant 13$) have been measured in the angular range 10°–50° for all the bombarding energies. This covered backward angles in the center-of-mass (c.m.) frame, because of the inverse kinematics of the reactions. Typical energy spectra of the emitted fragments ($3 \leqslant Z \leqslant 13$) obtained at an angle 10° at E_{lab} = 170 MeV are shown in Fig. 1. It is evident that the energy spectra for lighter fragments ($3 \leqslant Z \leqslant 6$) exhibit strong peaking in energy. The peaks are nearly Gaussian in shape, having the centroid at the expected kinetic energies for the fission fragments obtained from the Viola systematics corrected by the corresponding asymmetry factors [31,32], these are shown by arrows in Fig. 1. The shapes of the energy spectra for the other heavier fragments ($7 \leqslant Z \leqslant 13$) are quite different from those obtained for the lighter ones. The additional contributions from DI and QE processes have been seen in the higher energy part of the spectra. Moreover, there are contributions from the recoiling nuclei (energy corresponding to $v_{CN} \cos\theta_{lab}$, shown by dashed lines in Fig. 1). All these contributions, other than fission fragments, fall off rapidly as one moves away from the grazing angle. In this article, we report the results from the lighter fragments (Z = 3–7).

The inclusive energy distributions for the fragments lithium (Z = 3), beryllium (Z = 4), boron (Z = 5), carbon (Z = 6), and nitrogen (Z = 7) obtained at an angle 10° at various

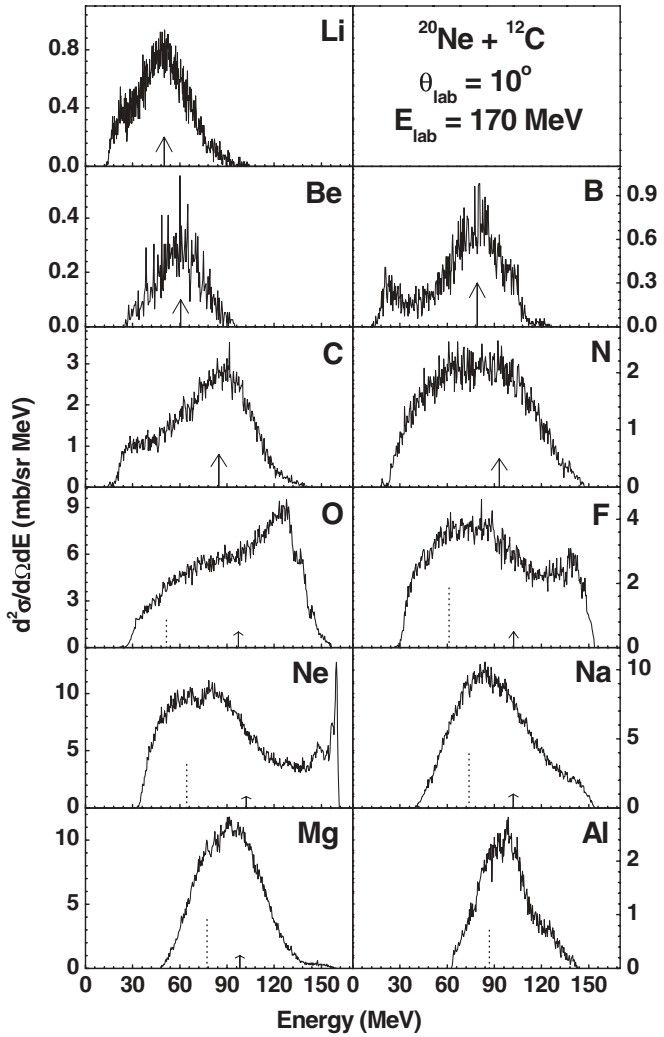

FIG. 1. Inclusive energy distributions of different fragments emitted in the reaction ^{20}Ne(170 MeV)+^{12}C at $\theta_{lab} = 10^{\circ}$. The arrow corresponds to the expected fission fragment kinetic energy. The dashed line indicates the average energy of the recoiling nucleus.

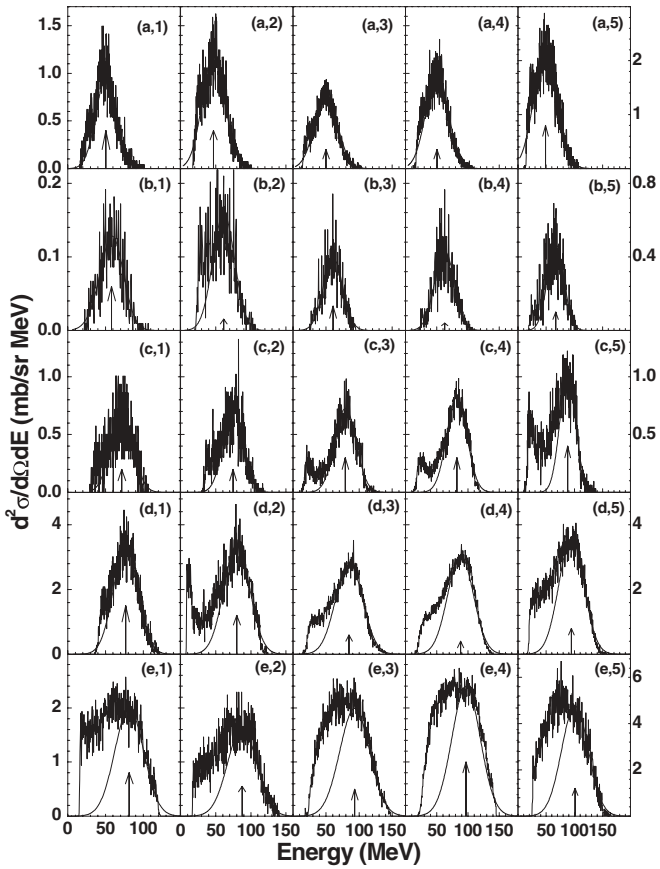

FIG. 2. Inclusive energy distributions for the fragments lithium (a), beryllium (b), boron (c), carbon (d), and nitrogen (e) emitted in the reaction ^{20}Ne+^{12}C at an angle 10° for bombarding energies 145 MeV (1), 158 MeV (2), 170 MeV (3), 180 MeV (4), and 200 MeV (5), respectively. The arrow corresponds to the centroid of the fitted Gaussian distribution (solid curve).

bombarding energies are shown in Fig. 2. It is observed that at all bombarding energies the energy spectra of the ejectiles (Li, Be, B, C, N) are nearly Gaussian in shape and they have been fitted with a single Gaussian. The non-Gaussian shapes at the low-energy side of the spectra correspond to sequential decay processes, which can be simulated by Monte Carlo statistical model calculations (described in Sec. IV A). The Gaussian fits so obtained are shown by solid lines in Fig. 2. The centroids (shown by arrows) are found to correspond to the scission of deformed dinuclear configuration [15,31,32]. This suggests that, in all cases, the fragments are emitted from fully energy relaxed composite—as expected for both FF and orbiting processes. The increasing yields at lower energies may also be due to the second kinematical solution, which is a signature of binary nature of emission process.

B. Average velocity

The average velocities of the fragments have been computed from the measured energies and from the Z values using the empirical relation proposed by Charity *et al*. [33]:

$$A = Z \times (2.08 + 0.0029 \times Z). \quad (1)$$

The average velocities of the fragments obtained at different bombarding energies have been plotted in the $v_{\parallel}$ vs. $v_{\perp}$ plane in Fig. 3. It is seen that at all energies, the average velocities of different fragments fall on a circle centered around the respective v_{CN}, the compound nuclear velocity. This suggests that at all bombarding energies the average velocities (as well as kinetic energies) of the fragments are independent of the c.m. emission angles and indicates that at all these energies the fragments are emitted from a fully equilibrated CN-like source with full momentum transfer. The magnitude of the average fragment velocities (i.e., the radii of the circles in Fig. 3) decreases with the increase of fragment mass, which is indicative of the binary nature of the emission.

C. Angular distribution

The center-of-mass angular distributions of the fragments (Li, Be, B, C, and N) emitted in the ^{20}Ne (145, 158, 170, 180, and 200 MeV) + ^{12}C reactions are shown in Fig. 4. The transformations from the laboratory to center-of-mass

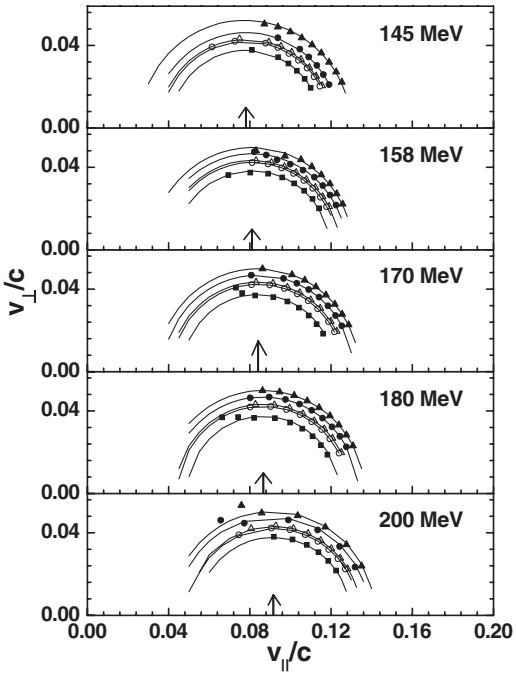

FIG. 3. The average velocities of the fragments plotted in $v_{\parallel}$ vs. $v_{\perp}$ plane at different bombarding energies. The average velocities are denoted by filled triangles (Li), filled circles (Be), open triangles (B), open circles (C), and filled squares (N). The arrows correspond to the compound nucleus velocities.

system have been done with the assumption of a two body kinematics averaged over total kinetic energy distributions. The center-of-mass angular distributions of these fragments obtained at all bombarding energies follow the $1/\sin\theta_{\text{c.m.}}$-like variation (shown by solid lines in Fig. 4), which further

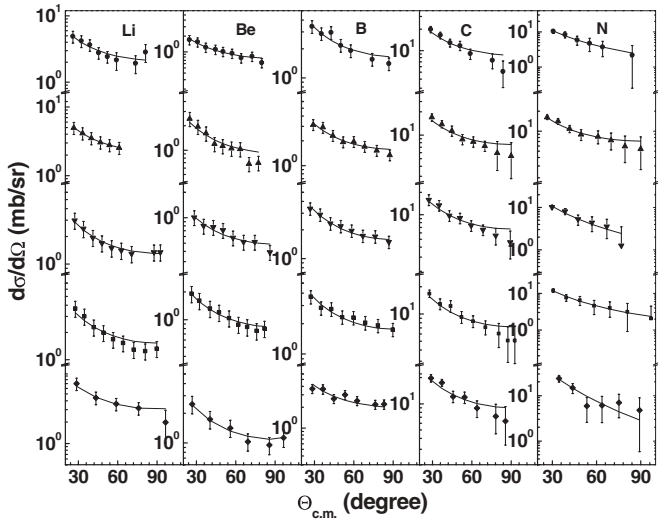

FIG. 4. The center-of-mass angular distributions of fragments ($Z = 3$–7) obtained at different bombarding energies. Solid circles (145 MeV), triangles (158 MeV), inverted triangles (170 MeV), squares (180 MeV), and diamonds (200 MeV) correspond to the experimental data and the solid lines are $f(\theta_{\text{c.m.}}) \sim 1/\sin\theta_{\text{c.m.}}$ fit to the data.

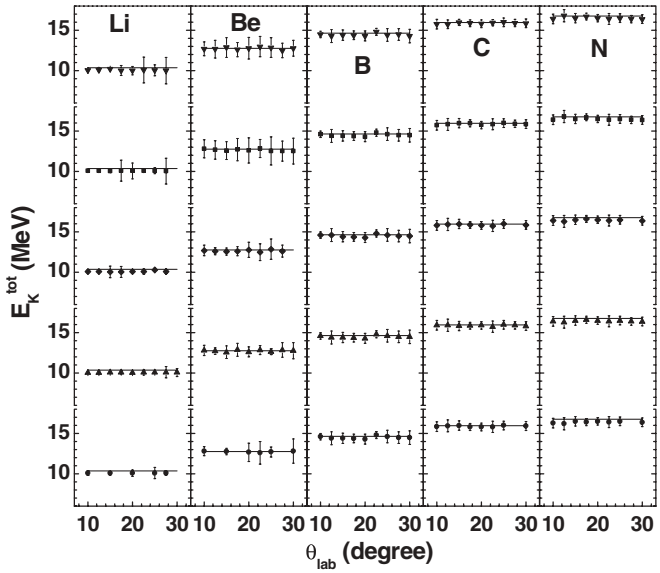

FIG. 5. Average kinetic energy of different fragments obtained at $E_{\text{lab}} = 145$, 158, 170, 180, and 200 MeV (denoted by inverted triangle, square, diamond, triangle, and circle, respectively) plotted as a function of laboratory angle.

corroborate the conjecture of emission from fully equilibrated composite.

D. Average kinetic energy

The average total kinetic energies in the center-of-mass, E_K^{tot}, for the fragments ($3 \leqslant Z \leqslant 7$) obtained at all bombarding energies, have been displayed as a function of scattering angle in Fig. 5. The average fragment kinetic energies in the center-of-mass have been obtained from the respective laboratory values assuming two body kinematics. It is observed from Fig. 5 that E_K^{tot} values are almost constant for each of the exit channel. The near constancy of E_K^{tot} indicates that at all energies the lifetime of the dinuclear complex is longer than the time needed to completely damp the energy in the relative motion [34–37]. The predictions of Viola systematics [31] for fission fragment kinetic energies, corrected by an asymmetric factor [32], have been shown by solid lines in Fig. 5. The E_K^{tot} values predicted from Viola systematics are found to be in good agreement with the experimental data at all bombarding energies.

E. Average Q-value distribution

The variations of average Q value, $\langle Q \rangle$, with center-of-mass emission angle for the fragments Li, Be, B, C, and N obtained at different bombarding energies are shown in Fig. 6. It is observed that the $\langle Q \rangle$ of different fragments are independent of the center-of-mass emission angles at all bombarding energies. This is in contrast to the observation made earlier for other light systems [^{16}O (116 MeV)+^{27}Al, ^{28}Si, ^{20}Ne (145 MeV)+^{27}Al, ^{59}Co systems], where sharp falloff of $\langle Q \rangle$ with angle have been seen [5,6]. The $\langle Q \rangle$ values remain nearly constant, which further suggests that at all angles, the fragments are emitted from completely equilibrated source at all incident energies considered here.

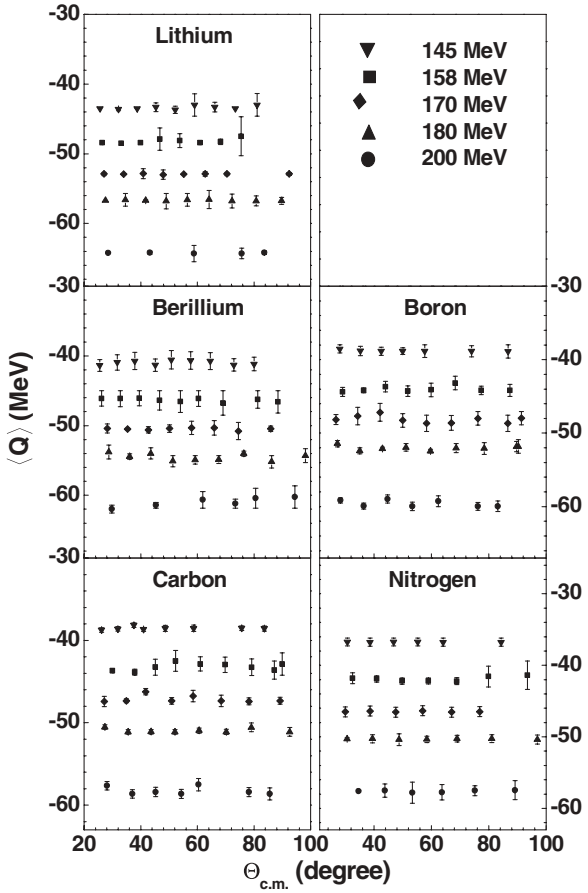

FIG. 6. Average Q values of different fragments obtained at $E_{lab} = 145$, 158, 170, 180, and 200 MeV (denoted by inverted triangle, square, diamond, triangle, and circle, respectively) plotted as a function of center-of-mass emission angle.

F. Equilibrium cross section

The energy distributions, velocity diagrams, angular distributions and $\langle Q \rangle$ distributions indicate that the yield of these fragments ($Z = 3$–7) originates from fully energy relaxed events associated with the decay of either compound nucleus or long-lived, orbiting dinuclear system. A detailed investigation have been made to decipher the role played by aforementioned processes in the fragment yield by comparing the experimental yields with the theoretical predictions of the standard statistical model [38], extended Hauser-Feshbach model (EHFM) [20]. The experimental angle integrated yields of the fragments emitted in the ^{20}Ne+^{12}C reaction at different bombarding energies are shown in Fig. 7 by solid circles (taken from Ref. [13]) and triangles. The theoretical predictions of the statistical model code CASCADE [38] are shown by solid lines in Fig. 7. The calculations are done considering l values up to the critical angular momentum of fusion, l_{cr}, at each energy (given in Table I). It is observed that at all energies the experimental yields of the fragments Li and Be are in fair agreement with the theoretical CASCADE prediction. However, the yields of

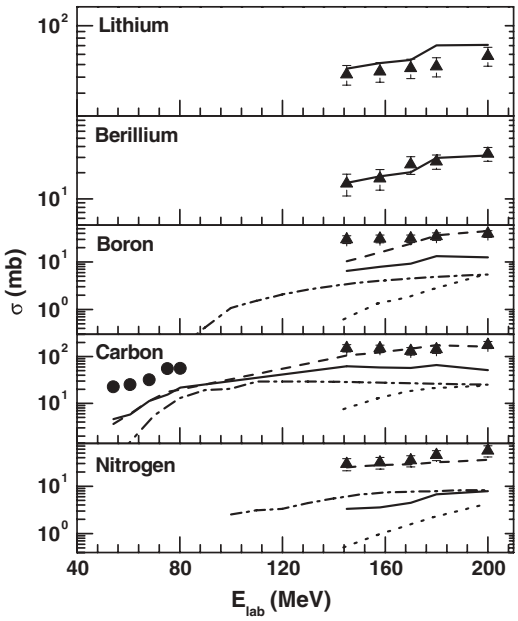

FIG. 7. The excitation functions for the angle-integrated yield of the fragments. Triangles are the present data; lower energy data (filled circles) for carbon fragments are taken from Ref. [13]. The solid curves are the predictions of the statistical model. The dash-dotted curves for B, C, and N are prediction of equilibrium orbiting model and the dotted curves are the same from EHFM [20]. The dashed curves show CASCADE calculations using grazing angular momentum.

TABLE I. The angular momentum values, NOC, and C fragment yield for different energies.

System	E_{lab} (MeV)	E^* (MeV)	l_{cr} ($\hbar$)	l_{gr} ($\hbar$)	NOC[a]	C yield (mb)	
						Expt.	CASCADE[b]
Ne+C	109.5	60	20	26	5.2	122.6[c]	35.7
Ne+C	145	73	24	31	4.5	151.9 ± 26.8	62.2
Ne+C	158	78	24	33	8.2	149.7 ± 26.5	58.7
Ne+C	170	82	24	34	11.0	131.8 ± 23.8	56.9
Ne+C	180	86	25	36	33.0	142.9 ± 25.4	66.0
Ne+C	200	94	25	38	73.2	178.3 ± 30.7	51.4
F+C	96	60	21	24	97.2	47.92 ± 4.37 [7]	34.5

[a]Values taken from Ref. [29].
[b]Calculation done using l_{cr} values given in Table I.
[c]Extracted from Fig. 7.

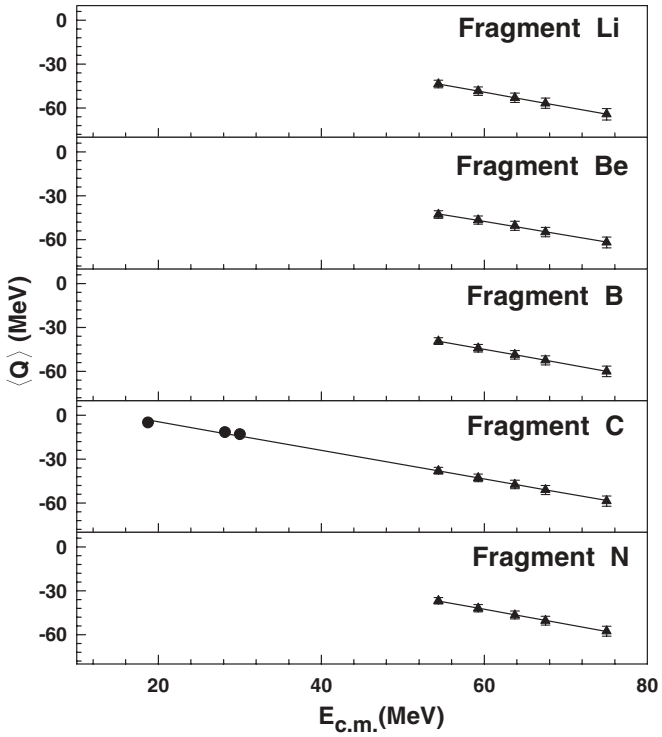

FIG. 8. Bombarding energy dependence of the average Q values. The solid line shows the linear dependence of $\langle Q \rangle$ with bombarding energy. The $\langle Q \rangle$ values at lower energies for carbon are taken from Ref. [13].

the fragments B, C, and N (near entrance channel) obtained at different energies are much higher than those predicted by the statistical model code CASCADE. A similar observation has been reported by Shapira *et al.* [12,13] for the same system at lower energies for carbon fragment. The theoretical predictions using EHFM have also been shown by dotted lines in Fig. 7 for the fragments B, C, and N. The EHFM predictions also similar to those obtained from CASCADE calculations and the experimental yields are in fair excess of the theoretical estimates of both CASCADE and EHFM.

G. Excitation energy dependence of $\langle Q \rangle$

The average Q values ($\langle Q \rangle$) for the fragments Li, Be, B, C, and N have been plotted in Fig. 8 as a function of the incident energy. The linear dependence of $\langle Q \rangle$ with energy provides strong evidence that the long lifetime may be associated with an orbiting phenomenon. This linear dependence of $\langle Q \rangle$ can be expressed by simple equation of the form $\langle Q \rangle = c - m^* E_{\mathrm{c.m.}}$, where m is the slope and c is the intercept [for example, $\langle Q \rangle = (14.9 \pm 1.0) - (0.97 \pm 0.02)\ \mathrm{E_{c.m.}}$ for the fragment carbon]. The experimentally determined intercepts are found to be in fair agreement with kinetic energies calculated using Viola systematics. It is interesting to note that the $\langle Q \rangle$ values obtained in the present experiment between 145 and 200 MeV fall on the same straight line extrapolated from the lower energy (∼54–81 MeV) data [13]. This means that the energy relaxation is complete for the fragment emission studied here up to the incident energy of 200 MeV. Moreover, it also means that the final kinetic energy ($\mathrm{E}^f_{\mathrm{kin}} = \langle Q \rangle + \mathrm{E_{c.m.}}$) is nearly independent of bombarding energy, which may be due to the limitation on the maximum value of angular momentum beyond which the formation of di-nucleus is not allowed due to centrifugal repulsion [24].

IV. DISCUSSIONS

In general, the energy distributions, the angular distributions, and the total fragment yields measured for ^{20}Ne+^{12}C reaction at incident energies between 145 and 200 MeV are similar to those obtained at lower incident energies (∼50–80 MeV) for the same system (see Refs. [12,13]). Large energy damping, $1/\sin\theta_{\mathrm{c.m.}}$ dependence of angular distribution and near constancy of $\langle Q \rangle$ over a wide angular range signify that the fragment decay originates from a long-lived, fully energy equilibrated system. However, the large enhancement of fragment emission cross section ($5 \leqslant Z \leqslant 7$) over the statistical-model predictions leads to the conjecture that the orbiting mechanism may still play a major role at these energies. The possibility of these enhancements, due to either feeding from the secondary de-excitation of the heavier fragments or orbiting mechanism, are investigated in great details and described in the following subsections.

A. Contribution from secondary decay of heavier fragments

There is a possibility that the primary heavier fragments (formed due to the binary decay of composite system) may have sufficient excitation energy to de-excite through the emission of light particles and γ rays and contribute to the yield of lighter fragments. This additional contribution from the secondary decay increases the total elemental yield of the lighter fragments. To check whether the enhancement in B, C, and N yield could be due to feeding from the secondary decay of heavier fragments of various possible binary breakup combinations, we have performed detailed simulations of secondary decay using the Monte Carlo binary decay version of the statistical decay code LILITA [39] and the statistical model code CASCADE [38] and PACE4 [40]. Secondary decay of Si* (binary channel ^{28}Si+^{4}He), Al* (binary channel ^{26,25}Al+^{6,7}Li), Mg* (binary channel ^{24,25,23}Mg+^{8,7,9}Be), Na* (binary channel ^{22,21}Na+^{10,11}B), Ne* (binary channel ^{20}Ne+^{12}C), F* (binary channel ^{18}F+^{14}N), O* (binary channel ^{16}O+^{16}O), N* (binary channel ^{14}N+^{18}F), C* (binary channel ^{12}C+^{20}Ne), B* (binary channel ^{10,11}B+^{22,21}Na), and Be* (binary channel ^{8,7,9}Be+^{24,25,23}Mg) have been studied. Indeed the LILITA calculations (using the parameter set proposed in the Appendix of Ref. [13] and assuming the excitation energy division follows the mass ratio [1]) are in qualitative agreement with the experimental results obtained at 9 MeV/nucleon by Rae *et al.* [41] for the sequential decay of ^{20}Ne+^{12}C. It was found that even at the highest excitation energy, secondary decay of Si* and Al* do not reach up to N; the contribution of primary Mg*, Na* decay to $Z \leqslant 7$ were estimated to be $\lesssim$1% of the primary yield and that of Ne* decay to N, C, and B yield were estimated to be ∼10–20%, ∼15–20%, and ∼30–50%

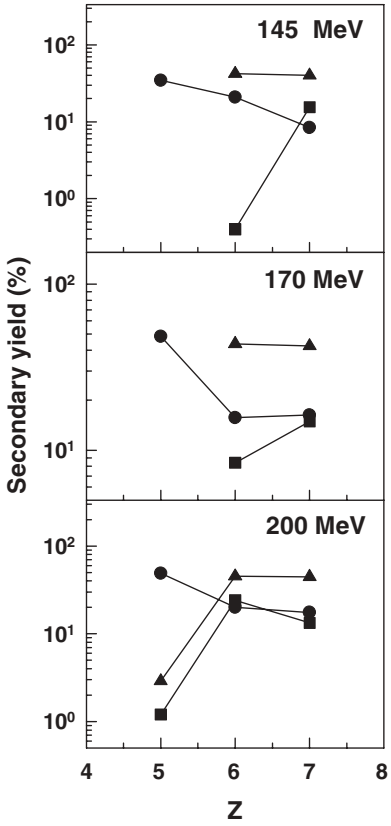

FIG. 9. Percentage secondary decay contribution from primary Ne* (circle), F* (square), and O* (triangle) to $Z = 5$–7.

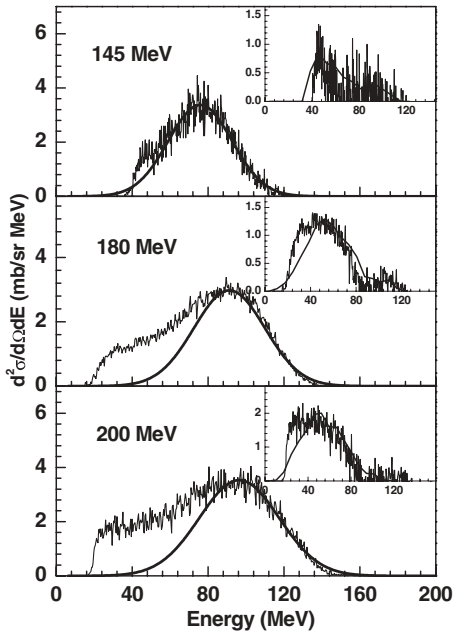

FIG. 10. Secondary decay contribution for carbon fragments at different energies. The energy distribution at $\theta_{lab} = 10^{\circ}$ along with the fitted Gaussian are shown. (Inset) Distribution shows the difference spectra (total spectra - Gaussian) and the solid line represents the total secondary decay contribution estimated using LILITA [39].

of the primary yield, respectively. Nearly ∼40–45% of the primary O* produced through binary exit channel $^{16}O+^{16}O$ decays to C. The secondary decay yields from the primary excited fragments are shown in Fig. 9 for different bombarding energies. As the binary yield of O and F are small (∼10% of the binary Ne yield, as estimated from CASCADE [38]), overall secondary decay contribution from O and F are smaller than that from Ne. Moreover, the simulations of energy distributions of the secondary decay yield of C from Ne as well as F and O using the code LILITA show that they peak at much lower energies (typically, at ∼45–50 MeV for Ne, ∼48–55 MeV for F, and ∼55–60 MeV for O, compared to the peak of the experimental energy distribution at ∼75–95 MeV).

Now, the Gaussian fitting procedure for the extraction of primary fragment yield is fairly efficient in rejecting most of the low energy tail (typical rejection ratio ∼25–40% of the total yield). The energy distributions of the secondary decay have been shown in Fig. 10 for carbon, in Fig. 11 for boron, and in Fig. 12 for nitrogen. In the inset of these figures the spectra shown are the difference spectra; the difference between the experimental spectra and the Gaussian fitted to the spectra. It has been found that the secondary decay distributions reproduce the difference spectra very well for all the cases. It is thus evident that the secondary decay component does not interfere with the estimated primary yield for two reasons: first, total secondary decay yield is not quite large, and second, the Gaussian fitting procedure for the extraction of primary yield does take care, to a large extent, of the rejection of the contributions of the secondary decay components as their energy distributions are different from those of the primary components.

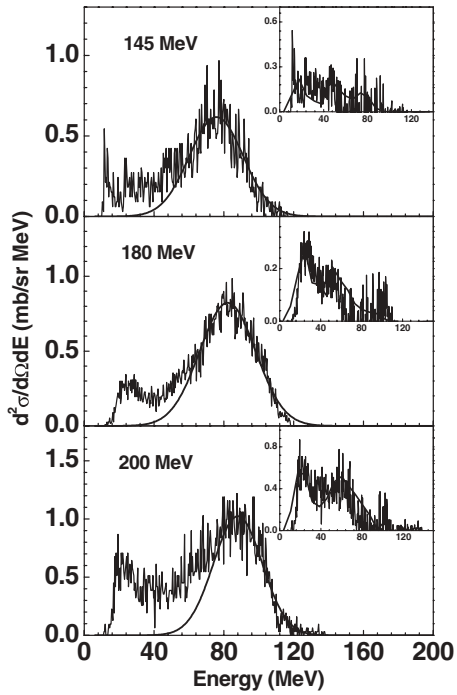

FIG. 11. Same as Fig. 10 for boron fragments.

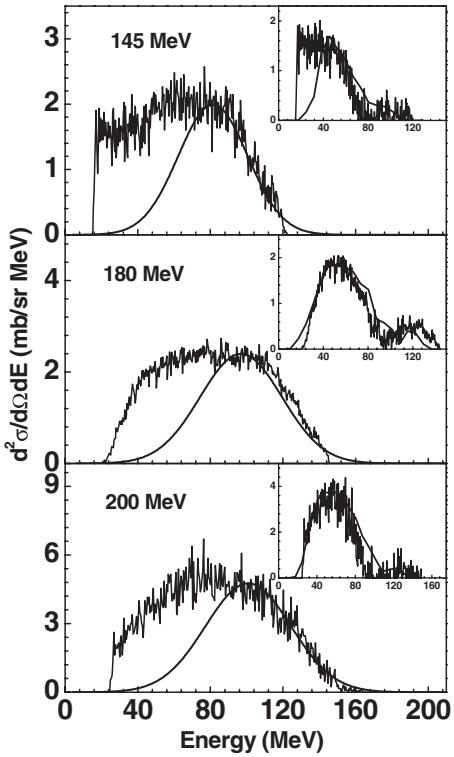

FIG. 12. Same as Fig. 10 for nitrogen fragments.

B. Fragment cross section

It has been observed that the statistical model calculations do not reproduce most of the observed experimental yields, therefore, an additional reaction component corresponding to the orbiting mechanism has to be considered. The large measured cross sections for B, C, and N fragments led to the suggestion that an orbiting, dinuclear configuration is formed that decays back to the entrance channel. After the discovery of orbiting in the $^{28}Si+^{12}C$ system, similar enhancements of large-angle, binary-reaction yields are also observed in the present data. It is expected that the orbiting mechanism will retain a greater memory of the entrance channel than the fusion-fission process. The trapped, dinuclear complex can either evolve with complete amalgamation into a fully equilibrated compound nucleus or, alternatively, escape into a binary exit channel by way of orbiting trajectories. Orbiting can therefore be described in terms of the formation of a long-lived dinuclear molecular complex that acts as a "doorway" state to fusion with a strong memory of the entrance channel. The equilibrium orbiting model has been used to successfully explain both the observed cross sections and total kinetic energy (TKE) values of the fully damped fragments for several lighter nuclear systems at lower energies. The theoretical prediction of the equilibrium model for orbiting and fusion [15] is denoted by dash-dotted line in Fig. 7 for the fragment B, C, and N, and it also fails to explain the large enhancement in the fragment yield. The curve displayed in Fig. 7 represents the "best fit" that can be obtained by the orbiting model with a reasonable choice of the Bass potential parameters (strengths, short range, and long range of the proximity potential). It is, therefore, evident that both the equilibrium orbiting and statistical decay (CASCADE, EHFM) models result in comparable disagreement with the data. It may be interesting to note here that Shapira *et al.* studied the same reaction at lower energies [12,13] and came to the conclusion that the large enhancements in the energy damped fragment yield observed at those energies might be due to nuclear orbiting phenomenon.

The shortcomings of the equilibrium model for orbiting does not imply that the presence of an orbiting mechanism, as distinct from fission, can be ruled out. On the contrary, there may be a large orbiting-like contribution from non fusion window (in the angular momentum window $l_{cr} \leqslant l \leqslant l_{gr}$). This is consistent, at least qualitatively, with the fact that the CASCADE calculation [38] performed with l values up to l_{gr} (shown by dashed lines in Fig. 7) is found to reproduce the data fairly well. The values of l_{gr} at different bombarding energies are given in Table I. Yields in the transfer channels (B and N, for example) are also found to be strongly affected by the orbiting process (yield enhancement), which may be due to stochastic nucleon exchanges during long lifetime of the dinuclear system.

In Fig. 13, we show the ratio of beryllium to lithium (square), boron, to lithium (circle), carbon to lithium (triangle), and nitrogen to lithium (inverted triangle) yield as a function of bombarding energies and the corresponding statistical-model (CASCADE) calculations (solid lines). It is found that the observed beryllium to lithium ratio is well explained with the statistical-model calculations. However, the other observed ratios are higher than the theoretically calculated ratios. This implies the dominance of orbiting yield over the compound nucleus yield.

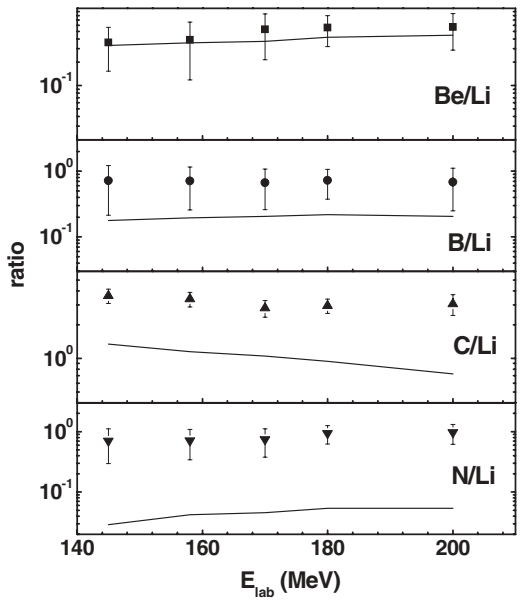

FIG. 13. Bombarding energy dependence of the ratio of angle-integrated fragment yield. The beryllium to lithium (square), boron to lithium (circle), carbon to lithium (triangle), and nitrogen to lithium (inverted triangle) ratios are shown. The solid line shows the theoretical prediction using CASCADE.

C. Comparison of the ^{20}Ne+^{12}C and ^{19}F+^{12}C reactions

The large orbiting yields that account for the largest part of the fully damped yields of ^{20}Ne+^{12}C can be qualitatively understood in the framework of the number of open channels (NOC) model [29,42]. The calculated NOC are shown in Table I for both the ^{20}Ne+^{12}C and the ^{19}F+^{12}C reactions [29] at several excitation energies along with the measured and calculated (fusion-fission cross sections as predicted by CASCADE) fully damped yields. The NOC for ^{20}Ne+^{12}C exhibits the characteristic minimum for a grazing angular momentum of approximately $l_{gr} = 30\hbar$ [29]. This very deep minimum (NOC = 4.5) explains (i) why resonant structures have been observed to be significant in ^{20}Ne+^{12}C [27,28] and (ii) why the orbiting yields observed for C fragments are much larger than the CASCADE predictions. The comparison with ^{19}F+^{12}C is instructive at $E^* = 60$ MeV [7] (the corresponding value of the yield of fragment C for ^{20}Ne+^{12}C, as given in Table I, has been extracted from Fig. 7 to permit a direct comparison with ^{19}F+^{12}C). The large NOC value for ^{19}F+^{12}C [29] (almost order of magnitude bigger) is consistent with the fact that essentially no resonances have been observed in this system [43,44]. This was confirmed by the time-scale measurements of Suaide *et al.* [45], who found that fusion-fission (with high NOC values), a very slow mechanism, is more competitive than a faster process such as orbiting (with small NOC values) in ^{19}F+^{12}C. It is worth noting from Table I that CASCADE predicts almost identical fusion-fission cross section for both reactions at $E^* = 60$ MeV. However, due to the survival of orbiting at energies larger than 7 MeV/nucleon, the fully damped yields are much more than a factor of two bigger for the ^{20}Ne+^{12}C system at $E^* =$ 60 MeV.

V. SUMMARY AND CONCLUSIONS

The inclusive double differential cross-section for fragments having $Z = 3$–7 emitted in the reaction ^{20}Ne (∼7–10 MeV/nucleon)+^{12}C have been measured. Total emission cross-section for the fragments Li to N have been estimated from the experimental distributions. The center-of-mass angular distributions for the fragments at all the bombarding energies are found to have a $1/\sin\theta_{\mathrm{c.m.}}$-type of dependence that signifies the emission of these fragments from a long-lived equilibrated composite. The average velocity plots in $v_\parallel$ vs. $v_\perp$ plane indicate that the fragments are emitted from fully equilibrated source moving with compound nucleus velocity. The average kinetic energy and the average Q value of the fragments are independent of the emission angles. This also suggests the emission from a long-lived, equilibrated composite. The angle-integrated cross section for Li and Be fragments agree well with the theoretical predictions of statistical model but the yield of B, C, and N fragments (near to entrance channel) are in excess with the theoretically predicted values. This indicates the presence of other type of reaction process, namely orbiting. In contrast, the study of the nearby system ^{19}F (96 MeV)+^{12}C clearly showed that the fragments are emitted in the fusion-fission process [7]. Low values of NOC [29] obtained for ^{20}Ne+^{12}C system as compared to the same obtained for ^{19}F+^{12}C system also confirms the conjecture of survival of orbiting in ^{20}Ne+^{12}C system at higher excitations. It is interesting to mention at this point that ^{16}O, ^{20}Ne+^{28}Si systems [6,10,11], even though α-like, do not show the characteristics of orbiting at these energies, but orbiting-like behavior has been observed for ^{28}Si+^{16}O reaction at lower energies [22].

The present analysis also indicates that the enhancement in fragment yield for ^{20}Ne+^{12}C reactions cannot be explained by the equilibrium orbiting model [15]. This may be due to the fact that the equilibrium orbiting model in its present form seems to be inadequate to explain the phenomena at higher excitations, and a more complete understanding of orbiting and via the angular momentum dissipation (which plays a crucial role in defining orbiting trajectories and yield) will be required.

ACKNOWLEDGMENTS

The authors thank the cyclotron operating crew for smooth running of the machine and H. P. Sil for the fabrication of thin silicon detectors for the experiment. One of the authors (A.D.) acknowledges with thanks the financial support provided by the Council of Scientific and Industrial Research, Government of India.

[1] S. J. Sanders, A. Szanto de Toledo, and C. Beck, Phys. Rep. **311**, 487 (1999) and references therein.
[2] N. Carlin Filho *et al.*, Phys. Rev. C **40**, 91 (1989).
[3] S. J. Padalino *et al.*, Phys. Rev. C **41**, 594 (1990).
[4] C. Bhattacharya *et al.*, Phys. Rev. C **72**, 021601(R) (2005).
[5] C. Bhattacharya *et al.*, Phys. Rev. C **66**, 047601 (2002).
[6] C. Bhattacharya *et al.*, Phys. Rev. C **69**, 024607 (2004).
[7] C. Bhattacharya *et al.*, Phys. Rev. C **54**, 3099 (1996).
[8] C. Beck *et al.*, Eur. Phys. J. A **2**, 281 (1998).
[9] C. Beck *et al.*, Phys. Rev. C **54**, 227 (1996).
[10] S. P. Barrow *et al.*, Phys. Rev. C **52**, 3088 (1995).
[11] K. Farrar *et al.*, Phys. Rev. C **54**, 1249 (1996).
[12] D. Shapira, J. L. C. Ford, Jr., J. Gomez del Campo, R. G. Stokstad, and R. M. DeVries, Phys. Rev. Lett. **43**, 1781 (1979).
[13] D. Shapira, J. L. C. Ford, Jr., and J. Gomez del Campo, Phys. Rev. C **26**, 2470 (1982).
[14] D. Shapira, R. Novotny, Y. C. Chan, K. A. Erb, J. L. C. Ford, jr., J. C. Peng, and J. D. Moses, Phys. Lett. **B114**, 111 (1982).
[15] B. Shivakumar, S. Ayik, B. A. Harmon, and D. Shapira, Phys. Rev. C **35**, 1730 (1987).
[16] W. Dünnweber *et al.*, Phys. Rev. Lett. **61**, 927 (1988).
[17] Aparajita Dey, C. Bhattacharya, S. Bhattacharya, T. K. Rana, S. Kundu, K. Banerjee, S. Mukhopadhyay, S. R. Banerjee, D. Gupta, and R. Saha, Phys. Rev. C **75**, 064606 (2007).
[18] L. G. Moretto, Nucl. Phys. **A247**, 211 (1975).
[19] S. J. Sanders, Phys. Rev. C **44**, 2676 (1991).
[20] T. Matsuse, C. Beck, R. Nouicer, and D. Mahboub, Phys. Rev. C **55**, 1380 (1997).

[21] A. K. Dhara, C. Bhattacharya, S. Bhattacharya, and K. Krishan, Phys. Rev. C **48**, 1910 (1993).
[22] A. Szanto de Toledo, S. J. Sanders, and C. Beck, Phys. Rev. C **56**, 558 (1997).
[23] A. Szanto de Toledo, B. V. Carlson, C. Beck, and M. Thoennessen, Phys. Rev. C **54**, 3290 (1996).
[24] D. Shapira, D. Schull, J. L. C. Ford, Jr., B. Shivakumar, R. L. Parks, R. A. Cecil, and S. T. Thornton, Phys. Rev. Lett. **53**, 1634 (1984).
[25] A. Gobbi *et al*., Phys. Rev. C **7**, 30 (1973).
[26] D. G. Kovar *et al*., Phys. Rev. C **20**, 1305 (1979).
[27] J. J. Kolata, R. C. Fuller, R. M. Freeman, F. Haas, B. Heusch, and A. Gallmann, Phys. Rev. C **16**, 891 (1977).
[28] I. Tserruya, Y. Eisen, D. Pelte, A. Gavron, H. Oeschler, D. Berndt, and H. L. Harney, Phys. Rev. C **18**, 1688 (1978).
[29] C. Beck, Y. Abe, N. Aissaoui, B. Djerroud, and F. Haas, Phys. Rev. C **49**, 2618 (1994).
[30] J. M. Oliveira *et al*., Phys. Rev. C **53**, 2926 (1996).
[31] V. E. Viola, K. Kwiatkowski, and M. Walker, Phys. Rev. C **31**, 1550 (1985).
[32] C. Beck *et al*., Z. Phys. A **343**, 309 (1992).
[33] R. J. Charity *et al*., Nucl. Phys. **A476**, 516 (1988).
[34] R. Eggers, M. N. Namboodri, P. Gonthier, K. Geoffroy, and J. B. Natowitz, Phys. Rev. Lett. **37**, 324 (1976).
[35] P. Braun-Munzinger, T. M. Cormier, and C. K. Gelbke, Phys. Rev. Lett. **37**, 1582 (1976).
[36] T. M. Cormier, P. Braun-Munzinger, P. M. Cormier, J. W. Harris, and L. L. Lee, Jr., Phys. Rev. C **16**, 215 (1977).
[37] J. B. Natowitz, M. N. Namboodri, R. Eggers, P. Gonthier, K. Geoffroy, R. Hanus, C. Towsley, and K. Das, Nucl. Phys. **A277**, 477 (1977).
[38] F. Pühlhofer, Nucl. Phys. **A280**, 267 (1977).
[39] J. Gomez del Campo and R. G. Stokstad, LILITA, a Monte Carlo Hauser-Feshbach code, ORNL-TM 7295.
[40] A. Gavron, Phys. Rev. C **21**, 230 (1980).
[41] W. D. M. Rae, A. J. Cole, B. G. Harvey, and R. G. Stokstad, Phys. Rev. C **30**, 158 (1984).
[42] C. Beck, Y. Abe, N. Aissaoui, B. Djerroud, and F. Haas, Nucl. Phys. **A583**, 269 (1995).
[43] N. Aissaoui, F. Haas, R. M. Freeman, C. Beck, A. Morsad, B. Djerroud, R. Caplar, G. A. Monnehan, A. Hachem, and M. Youlal, Z. Phys. A **348**, 237 (1994).
[44] N. Aissaoui, F. Haas, R. M. Freeman, C. Beck, A. Morsad, B. Djerroud, R. Caplar, and A. Hachem, Phys. Rev. C **55**, 516 (1997).
[45] A. A. P. Suaide *et al*., Phys. Rev. C **66**, 014607 (2002).